RSC Advances

PAPER

View Article Online
View Journal | View Issue

Cite this: *RSC Adv.*, 2024, **14**, 13900

Evaluation of ferroelectricity in a distorted wurtzite-type structure of Sc-doped $LiGaO_2$†

Sou Yasuhara, *[a] Ayato Nakagawa,[a] Kazuki Okamoto,[b] Takahisa Shiraishi,[b] Hiroshi Funakubo,[b] Shintaro Yasui,[cd] Mitsuru Itoh,[e] Takaaki Tsurumi[a] and Takuya Hoshina[a]

Received 26th March 2024
Accepted 22nd April 2024

DOI: 10.1039/d4ra02296c

rsc.li/rsc-advances

Since the discovery of ferroelectricity in a wurtzite-type structure, this structural type has gathered much attention as a next-generation ferroelectric material due to its high polarization value combined with its high breakdown strength. However, the main targets of wurtzite-type ferroelectrics have been limited thus far to simple nitride/oxide compounds. The investigation of new ferroelectric materials with wurtzite-type structures is important for understanding ferroelectricity in such structures. We therefore focus on β-$LiGaO_2$ in this study. Although AlN and ZnO possess well-known wurtzite-type structures ($P6_3mc$), β-$LiGaO_2$ has a distorted wurtzite-type structure ($Pna2_1$), and there are no reports of ferroelectricity in $LiGaO_2$. In this study, we have revealed that $LiGaO_2$ exhibits relatively high barrier height energy for polarization switching, however, Sc doping effectively reduces that energy. Then, we conducted thin film preparation and evaluation for Sc-doped $LiGaO_2$ to observe its ferroelectric properties. We successfully observed ferroelectric behavior by using piezoresponse force microscopy measurements for $LiGa_{0.8}Sc_{0.2}O_2/SrRuO_3/(111)SrTiO_3$.

Wurtzite-type ferroelectrics have attracted much attention since the discovery of Sc-doped AlN exhibiting a high polarization value of over 100 μC cm^{-2}.[1] The wurtzite-type structure was well known as a pyroelectric material due to its high energy barrier for polarization switching.[2–4] In this structure, all cations occupy tetrahedral sites and pass through the oxygen-stuffed layer during polarization switching.[5,6] Ferroelectric behaviors have been reported thus far in Sc-doped AlN,[1,7] B-doped AlN,[8,9] Sc-doped GaN,[10,11] and Mg-doped ZnO.[12] Chemical doping into a wurtzite-type structure reduces the barrier energy of polarization switching, resulting in ferroelectricity. In the case of Sc-doped AlN, the polarization switching barrier energy was calculated as 0.12 eV.[13] In previous reports, strain effects for Sc-doped AlN,[14,15] doping level dependence in Sc-doped AlN[16] and ferroelectricity predictions of other new wurtzite-type material such as LaN,[17] Mg_2XN_3 (X = Sb, Ta and Nb)[18] and other complex materials[19] are demonstrated by using first-principles calculations. Although wurtzite-type ferroelectric materials are candidates for next-generation ferroelectric materials, ferroelectric observations in such structures have been limited to simple oxides/nitrides with chemical doping due to the relatively high barrier energy for polarization switching.[20] The limited selectivity of doping elements is attributed to the composition of simple oxides/nitrides, which consist of divalent/trivalent cations. In addition, there are limited options for new simple oxides/nitrides to be considered as ferroelectric materials.[4,17–19] Therefore, we have tried to investigate complex oxide materials with wurtzite-type related structures.

We focus on β-$LiGaO_2$, which exhibits a distorted wurtzite-type structure. The crystal structure of β-$LiGaO_2$ falls within the orthorhombic system with a space group of $Pna2_1$, and spontaneous polarization takes place along the *c*-axis.[21,22] A single crystal growth of β-$LiGaO_2$ was reported to serve as a substrate on which to deposit GaN thin films.[23,24] Due to the difference in ionic radii between Li^+ and Ga^{3+},[25] the tetrahedra are distorted compared to those in the wurtzite-type structure. Moreover, the selectivity in doping elements is improved because of the presence of monovalent and trivalent cations in the structure. $NaGaO_2$, $AgGaO_2$, and $CuGaO_2$ are reported to possess the same structure as β-$LiGaO_2$.[26–28] However, it is difficult to treat $NaGaO_2$ in air due to its high deliquescence. Besides, the synthesis of $AgGaO_2$ and $CuGaO_2$ requires $NaGaO_2$ as a starting material. Therefore, we decided to investigate the ferroelectricity in β-$LiGaO_2$. In this study, we carried out first-

[a]*School of Materials and Chemical Technology, Tokyo Institute of Technology, 2-12-1 Ookayama, Meguro-ku, Tokyo 152-8550, Japan. E-mail: yasuhara.s.aa@m.titech.ac.jp*
[b]*School of Materials and Chemical Technology, Tokyo Institute of Technology, 4259 Nagatsuta, Midori-ku, Yokohama, Kanagawa 226-8501, Japan*
[c]*Laboratory for Zero-Carbon Energy, Tokyo Institute of Technology, 2-12-1 Ookayama, Meguro-ku, Tokyo 152-8550, Japan*
[d]*Laboratory for Materials and Structures, Tokyo Institute of Technology, 4259 Nagatsuta, Midori-ku, Yokohama, Kanagawa 226-8503, Japan*
[e]*Office of Campus Management, Tokyo Institute of Technology, 4259 Nagatsuta, Midori-ku, Yokohama, Kanagawa 226-8501, Japan*

† Electronic supplementary information (ESI) available. See DOI: https://doi.org/10.1039/d4ra02296c

principles calculation and thin film preparation to evaluate a polarization switching of $LiGaO_2$ system. First, we revealed that non-doped $LiGaO_2$ showed relatively high barrier height energy for the polarization switching. Then, we carried out calculation to evaluate the effect of Ga-site substitution on $LiGaO_2$. The results suggested that Sc-doping effectively reduces that energy. Finally, we prepared Sc-doped $LiGaO_2$ epitaxial thin films and uncovered the probability of ferroelectricity using piezoresponse force microscopy (PFM).

We carried out density functional theory (DFT) calculations using the projector augmented wave (PAW) method[29] as implemented in the VASP[30,31] for structural optimizations. We utilized the modified Perdew–Burke–Ernzerhof generalized gradient approximation (PBEsol-GGA)[32] as the exchange–correlation functional in our calculations. The *k*-point mesh was $8 \times 8 \times 8$. The cutoff energy and convergence energy were 550 eV and 1.0×10^{-7} eV, respectively. Born effective charges were calculated using density functional perturbation theory (DFPT). The spontaneous polarization value was estimated as the product of Born effective charges and atomic displacements. The calculated crystal structure is depicted by using VESTA software.[33]

All thin films were fabricated *via* a pulsed laser deposition method with a fourth harmonic wavelength of Nd:YAG. First, we prepared a ceramics target of $Li(Ga_{1-x}Sc_x)O_2$ ($x = 0$, 0.05, 0.15, 0.20). The starting materials of Li_2CO_3, Ga_2O_3, and Sc_2O_3 were weighed through stoichiometry and well ground with an agate pestle and mortar. The powder was calcined at 740 °C for 12 h. After the calcination, the powder was pelletized by using a cold isostatic press of 200 MPa, and the prepared pellets were sintered at 1100 °C for 2 h. We then deposited $LiGaO_2$ film onto (111)$SrTiO_3$ using the sintered target. The deposition conditions were a substrate temperature of 500 °C and an oxygen partial pressure of 10 mTorr. The crystal structure of prepared thin films was evaluated using HR-XRD (Smartlab, Rigaku). For the evaluation of ferroelectricity, a conductive $SrRuO_3$ was deposited as a bottom electrode. The $SrRuO_3$ film was deposited at the substrate temperature of 650 °C and oxygen partial pressure of 50 mTorr. The ferroelectricity of the prepared films was evaluated using PFM (MFP-3D, Asylum Research).

The crystal structure of β-$LiGaO_2$ ($Pna2_1$) is shown in Fig. 1a. Using this polar structure as the reference, we created an intermediate structure representing polarization switching, where all cations moved in the [00−1] direction and occupied five-coordinate sites.[3,14,16] Fig. 1b and c show the crystal structures of the polar and intermediate states, respectively, after the structural optimization. The difference in final energy per formula unit between the polar and intermediate structures is 0.64 eV per f.u. This value is quite high compared with the 0.35 eV per f.u. in the Sc-doped AlN cases,[13] indicating that it is hard to observe ferroelectricity in non-doped $LiGaO_2$. We then focused on Ga^{3+} site substitution by trivalent cations (Al^{3+}, B^{3+}, Sc^{3+}). These three elements were selected in a viewpoint of ionic radii. The calculated unit cell has four Ga^{3+} sites. Replacing one Ga^{3+} site corresponds to a 25% doping level. The calculated structures with 25% Ga replaced $LiGaO_2$ by Al, B, and Sc are shown in Fig. S1.† The barrier height energies of Al-, B-, and Sc-doped $LiGaO_2$ are 0.55, 1.84, and 0.21 eV per f.u., respectively. These results suggest that Sc doping is particularly effective at reducing the barrier height energy for polarization switching.

We investigated the dependence of the Sc amount in the $LiGaO_2$ structure by using first-principles calculations. The crystal parameters after the structural optimization with Sc-doped $LiGaO_2$ (Sc-doped level: 0%, 25%, 50%, 75%, and 100%) are shown in Table 1, as are the average *u*-parameters. The *u*-parameter is the position of a cation-stuffed plane relative to an anion-stuffed plane along the polarization axis (*c*-axis) of a wurtzite-type structure. In a simple wurtzite-type structure, the structure is polar when the *u*-parameter is less than 0.5. In the case of a complex oxide with a wurtzite-type structure, there are more than two kinds of cations; thus, the cation-stuffed plane is not flat. We then evaluated the average *u*-parameters calculated for each cation site. The calculation results suggest that the *u*-parameters of the non-doped and 25% Sc-doped $LiGaO_2$ are less than 0.5. On the other hand, the *u*-parameters remain stable at 0.5 with Sc contents exceeding 50% in Sc-doped $LiGaO_2$. This

Table 1 Lattice parameters of calculated Sc-doped $LiGaO_2$ structures

	Sc0%	Sc25%	Sc50%	Sc75%	Sc100%
a (Å)	5.394	5.509	5.922	6.022	6.131
b (Å)	6.373	6.444	6.962	7.044	7.104
c (Å)	5.022	5.007	4.171	4.184	4.196
u (a.u.)	0.382	0.386	0.5	0.5	0.5

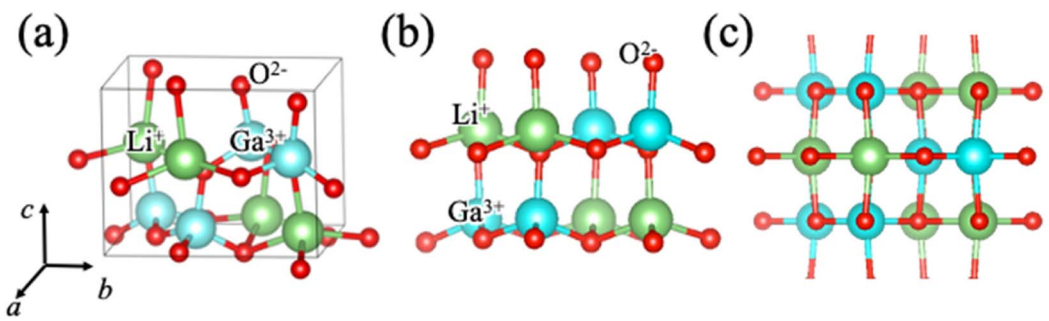

Fig. 1 (a) Schematic illustration of $LiGaO_2$ crystal structure. (b) The initial state of polarization switching and (c) the intermediate state of polarization switching in $LiGaO_2$.

result is attributed to the intermediate state of the polarization switching being more stable than the polar state. This result indicates that the intermediate state became stable as the Sc content increased in Sc-doped $LiGaO_2$. The same phenomenon was reported in Sc-doped AlN, where 50% Sc-doped AlN shows almost zero polarization value.[14] Besides, the *c*-axis length decreased with increasing Sc content in Sc-doped $LiGaO_2$. The polarization values calculated by using the DFPT method are 91.4 μC cm^{-2} (non-doped $LiGaO_2$) and 86.1 μC cm^{-2} ($LiGa_{0.75}Sc_{0.25}O_2$). The predicted polarization value is comparable to that in 90.0 μC cm^{-2} for ZnO,[5] and 90.6 μC cm^{-2} for Mg_2NbN_3.[18] Then, we have tried to prepare $LiGaO_2$ epitaxial thin films *via* a pulsed laser deposition method.

Fig. 2a shows the out-of-plane XRD results for the prepared thin films. β-$LiGaO_2$ ($Pna2_1$) *002* and *004* peaks were observed along the $SrTiO_3$[111] without any impurity peaks. This result indicates that the β-$LiGaO_2$ ($Pna2_1$)-oriented film is grown on the (111)$SrTiO_3$ substrate along the *c*-axis. Fig. 2b shows the results of phi-scan measurements on $LiGaO_2$ *011* and $SrTiO_3$ *110* to examine the crystal structure in the in-plane direction. Although a three-fold rotation symmetry is observed in $SrTiO_3$ *110*, a six-fold rotation is observed in $LiGaO_2$ *011* with a 30° peak shift from the $SrTiO_3$ *110* peaks. These results indicate that the in-plane relationship is $LiGaO_2$[010]//$SrTiO_3$[10−1], and the observed six-fold rotation symmetry of $LiGaO_2$ *011* appears to have originated from the three-fold rotation of (111)$SrTiO_3$. The result of 2D reciprocal space mapping of prepared $LiGaO_2$/(111)$SrTiO_3$ thin film is shown in Fig. S2.† The relationship of crystal orientation between (001)$LiGaO_2$ and (111)$SrTiO_3$ was depicted in Fig. S3.† Along $SrTiO_3$ [10−1] direction, $LiGaO_2$ is well matched with a lattice mismatch of 2.7%. The relationship of $LiGaO_2$/(111)$SrTiO_3$ is in good agreement with that of ZnO/(111)$SrTiO_3$,[34] although the space groups of ZnO is different with that of $LiGaO_2$ whereas the atomic alignment is same. There results indicated that (001)$LiGaO_2$/(111)$SrTiO_3$ epitaxial thin films were obtained. For electric measurements, $LiGaO_2$/$SrRuO_3$/(111)$SrTiO_3$ thin films were prepared by using $SrRuO_3$ as a bottom electrode. However, no ferroelectric behavior was observed *via* PFM (Fig. S4†) and *P*–*E* hysteresis measurements due to the relatively high barrier height energy of polarization switching in non-doped $LiGaO_2$. Therefore, we focused on Sc doping to Ga^{3+} sites in $LiGaO_2$.

$Li(Ga_{1-x}Sc_x)O_2$ (x = 0.05, 0.15, 0.20) ceramics targets were sintered by a conventional solid state reaction to prepare Sc-doped $LiGaO_2$ thin films. The XRD results of the prepared thin films are shown in Fig. 3a. $LiGaO_2$ *002* and $SrRuO_3$ $111_c/222_c$ peaks are observed along the out-of-plane direction, the same as in the non-doped $LiGaO_2$ epitaxial thin film. The *c*-axis length calculated from the out-of-plane XRD results are plotted in Fig. 3b. The calculated *c*-axis value is also shown in Fig. 3b. The *c*-axis length monotonically decreased as Sc content increased in Sc-doped $LiGaO_2$, indicating that Sc-doped $LiGaO_2$ epitaxial thin films were obtained. The result also suggests that the solution limit of Sc into $LiGaO_2$ epitaxial thin film is above 20%.

Finally, PFM results of $LiGa_{0.8}Sc_{0.2}O_2$/$SrRuO_3$/(111)$SrTiO_3$ are shown in Fig. 4a. We can clearly see a ferroelectric butterfly-shape curve of the amplitude signal and a 180° phase hysteresis curve. Additional PFM results measured in several points are shown in Fig. S5.† The result of non-doped $LiGaO_2$ epitaxial thin film is also shown in Fig. S4,† in which no ferroelectric behavior is observed. The results of written PFM images of phase and amplitude shown in Fig. 4b, which reflects a pre-imposed voltage before measurements. These findings suggest that the prepared thin film exhibits the potential for ferroelectric behavior. The frequency dependence of dielectric constant and dielectric loss of prepared sample is shown in Fig. S6.† The dielectric loss is less than 0.1 at 1 kHz. Unfortunately, we could not see a hysteresis loop in the *P*–*E* measurements because the prepared films were leaky during measurements applying high voltage. In our future studies, we intend to enhance the thin film quality by optimizing growth conditions. This will enable us to observe a *P*–*E* hysteresis loop, facilitating a direct evaluation of ferroelectricity in Sc-doped $LiGaO_2$.

We investigated ferroelectricity in $LiGaO_2$ by using calculation and preparation/evaluation of epitaxial thin films. We carried out first-principles calculations by using the VASP code for $LiGaO_2$ and Sc-doped $LiGaO_2$. The calculated results suggested that Sc doping reduces the barrier height energy of polarization switching in Sc-doped $LiGaO_2$. Then, we have

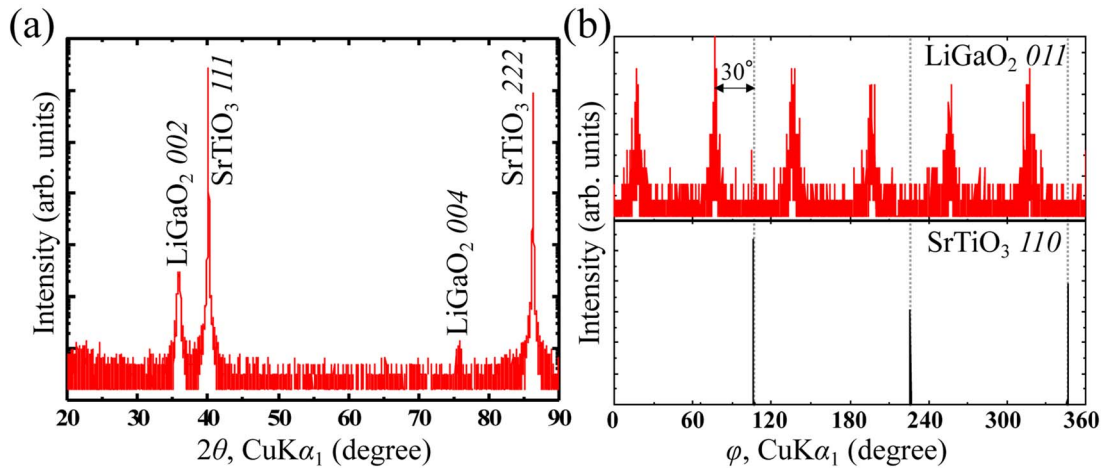

Fig. 2 (a) Out-of-plane XRD profiles of $LiGaO_2$/(111)$SrTiO_3$. (b) Phi-scan XRD patterns of $LiGaO_2$ *011* and $SrTiO_3$ *110*.

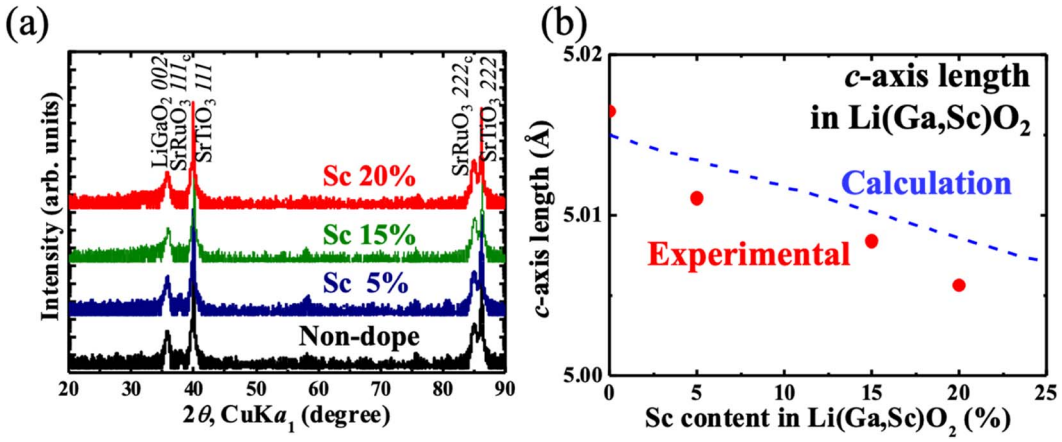

Fig. 3 (a) Out-of-plane XRD profiles of $LiGa_{1-x}Sc_xO_2$/(111)$SrTiO_3$ (x = 0, 0.05, 0.15, 0.20). (b) The c-axis lengths of prepared thin films with calculated values (blue dashed line).

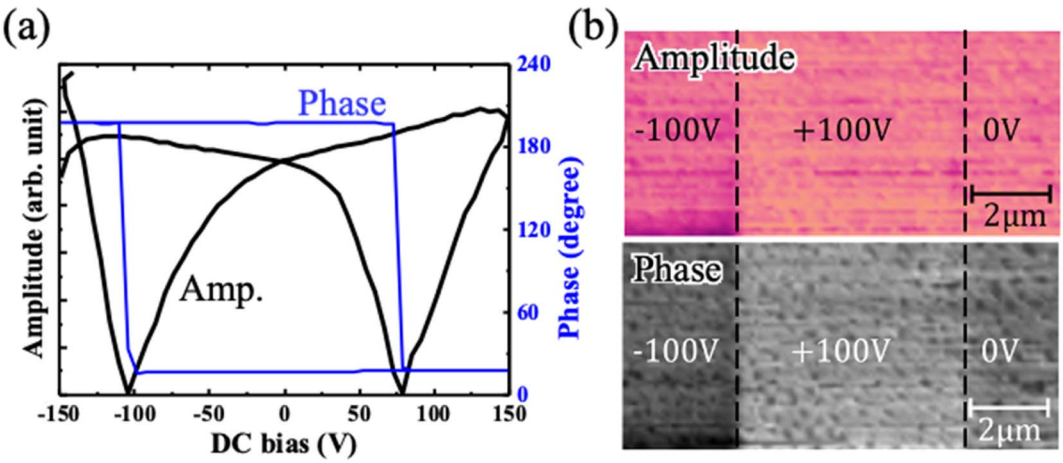

Fig. 4 (a) PFM results of amplitude (black line) and phase (blue line) signals in $LiGa_{0.8}Sc_{0.2}O_2$/$SrRuO_3$/(111)$SrTiO_3$. (b) PFM images of amplitude and phase for written sample in $LiGa_{0.8}Sc_{0.2}O_2$/$SrRuO_3$/(111)$SrTiO_3$.

started to prepare $LiGaO_2$ epitaxial thin film, and revealed that $LiGaO_2$ was epitaxially grown on a (111)$SrTiO_3$ substrate by a pulsed laser deposition method. The growth relationships between $LiGaO_2$ ($Pna2_1$) and the $SrTiO_3$ substrate are follows: (001)$LiGaO_2$//(111)$SrTiO_3$ and (010)$LiGaO_2$//(10−1)$SrTiO_3$. In this study, the pure $LiGaO_2$ does not show any ferroelectric behavior by using P–E measurements and PFM. We then prepared Sc-doped $LiGaO_2$ epitaxial thin films. We successfully observed ferroelectric behavior *via* PFM measurement for $LiGa_{0.8}Sc_{0.2}O_2$/$SrRuO_3$/(111)$SrTiO_3$.

Conflicts of interest

There are no conflicts to declare.

Acknowledgements

This study was partially supported by JSPS KAKENHI Grants-in-Aid for Research Activity Start-up (So. Y., 20K22549) and for Early-Career Scientists (So. Y., 22K14470), and by the Murata Science Foundation.

References

1 S. Fichtner, N. Wolff, F. Lofink, L. Kienle and B. Wagner, *J. Appl. Phys.*, 2019, **125**, 114103.
2 A. Konishi, T. Ogawa, C. A. J. Fisher, A. Kuwabara, T. Shimizu, S. Yasui, M. Itoh and H. Moriwake, *Appl. Phys. Lett.*, 2016, **109**, 102903.
3 Z. Liu, X. Wang, X. Ma, Y. Yang and D. Wu, *Appl. Phys. Lett.*, 2023, **122**, 122901.
4 H. Moriwake, R. Yokoi, A. Taguchi, T. Ogawa, C. A. J. Fisher, A. Kuwabara, Y. Sato, T. Shimizu, Y. Hamasaki, H. Takashima and M. Itoh, *APL Mater.*, 2020, **8**, 121102.
5 H. Moriwake, A. Konishi, T. Ogawa, K. Fujimura, C. A. J. Fisher, A. Kuwabara, T. Shimizu, S. Yasui and M. Itoh, *Appl. Phys. Lett.*, 2014, **104**, 242909.
6 L. Li and M. Wu, *ACS Nano*, 2017, **11**, 6382–6388.

7 K. H. Ye, G. Han, I. W. Yeu, C. S. Hwang and J.-H. Choi, *Phys. Status Solidi RRL*, 2021, **15**, 2100009.
8 W. Zhu, J. Hayden, F. He, J.-I. Yang, P. Tipsawat, M. D. Hossain, J.-P. Maria and S. Trolier-Mckinstry, *Appl. Phys. Lett.*, 2021, **119**, 062901.
9 J. Hayden, M. D. Hossain, Y. Xiong, K. Ferri, W. Zhu, M. V. Imperatore, N. Giebink, S. Trolier-McKinstry, I. Dabo and J.-P. Maria, *Phys. Rev. Mater.*, 2021, **5**, 044412.
10 D. Wang, P. Wang, B. Wang and Z. Mi, *Appl. Phys. Lett.*, 2021, **119**, 11902.
11 M. Uehara, R. Mizutani, S. Yasuoka, T. Shiraichi, T. Shimizu, H. Yamada, M. Akiyama and H. Funakubo, *Appl. Phys. Lett.*, 2021, **119**, 172901.
12 K. Ferri, S. S. Bachu, W. Zhu, M. Imperatore, J. Hayden, N. Alem, N. Giebink, S. Trolier-McKinstry and J.-P. Maria, *J. Appl. Phys.*, 2021, **130**, 044101.
13 H. Wang, N. Adamski, S. Mu and C. G. Van de Walle, *J. Appl. Phys.*, 2021, **130**, 104101.
14 S. Clima, C. Pashartis, J. Bizindavyi, S. R. C. McMitchell, M. Houssa, J. V. Houdt and G. Pourtois, *Appl. Phys. Lett.*, 2021, **119**, 172905.
15 D. F. Urban, O. Ambacher and C. Elsässer, *Phys. Rev. B*, 2021, **103**, 115204.
16 K. Furuta, K. Hirata, S. A. Anggraini, M. Akiyama, M. Uehara and H. Yamada, *J. Appl. Phys.*, 2021, **130**, 024104.
17 A. J. E. Rowberg, S. Mu, M. W. Swift and C. G. Van de Walle, *Phys. Rev. Mater.*, 2021, **5**, 094602.
18 X.-Y. Chen, J.-L. Yang, L.-F. Chen, H.-K. Xu, J.-M. Chen, G.-X. Lai, X.-F. Xu, H. Ji, J.-J. Tang and Y.-J. Zhao, *Phys. Chem. Chem. Phys.*, 2022, **24**, 29570–29578.
19 C.-W. Lee, N. U. Din, K. Yazawa, G. L Brennecka, A. Zakutayev and P. Gorai, *ChemRxiv*, 2023, preprint, DOI: 10.26434/chemrxiv-2023-hf60w.
20 Z. Liu, X. Wang, X. Ma, Y. Yang and D. Wu, *Appl. Phys. Lett.*, 2023, **122**, 122901.
21 M. Marezio, *Acta Crystallogr.*, 1965, **18**, 481.
22 C. A. Lenyk, M. S. Holston, B. E. Kananen, L. E. Halliburton and N. C. Giles, *J. Appl. Phys.*, 2018, **124**, 135702.
23 C. Chen, C.-A. Li, S.-H. Yu and M. M. C. Chou, *J. Cryst. Growth*, 2014, **402**, 325–329.
24 T. Ishii, Y. Tazoh and S. Miyazawa, *J. Cryst. Growth*, 1998, **186**, 409–419.
25 R. D. Shannon, *Acta Crystallogr.*, 1976, **A32**, 751–767.
26 I. Suzuki, A. Kakinuma, M. Uead and T. Omata, *J. Cryst. Growth*, 2018, **504**, 26–30.
27 H. Nagatani, I. Suzuki, S. Takemura, T. Ohsawa, N. Ohashi, S. Fujimoto and T. Omata, *AIP Adv.*, 2018, **8**, 085203.
28 I. Suzuki, H. Nagatani, M. Kita and T. Omata, *Appl. Phys. Express*, 2017, **10**, 095501.
29 P. E. Blöchl, *Phys. Rev. B: Condens. Matter Mater. Phys.*, 1994, **50**, 17953–17979.
30 G. Kresse and J. Furthmüller, *Phys. Rev. B: Condens. Matter Mater. Phys.*, 1996, **54**, 11169–11186.
31 G. Kresse and D. Joubert, *Phys. Rev. B: Condens. Matter Mater. Phys.*, 1999, **59**, 1758–1775.
32 J. P. Perdew, A. Ruzsinszky, G. I. Csonka, O. A. Vydrov, G. E. Scuseria, L. A. Constantin, X. Zhou and K. Burke, *Phys. Rev. Lett.*, 2008, **100**, 136406.
33 K. Momma and F. Izumi, *J. Appl. Crystallogr.*, 2011, **44**, 1272–1276.
34 Y. Zhan, J. Li, Y. Yin, W. Zhang and C. Jia, *RSC Adv.*, 2019, **8**, 37668–37674.